Peralkylated Ytterbium(II) Aluminate Complexes $YbAl_2R_8$. New Insights into the Nature of Aluminate Coordination

Michael G. Klimpel, Reiner Anwander,* Maxim Tafipolsky, and Wolfgang Scherer*

Anorganisch-chemisches Institut, Technische Universität München, D-85747 Garching, Lichtenbergstrasse 4, Germany

Received March 15, 2001

The homoleptic ytterbium(II) tetraalkylaluminate complexes $\{Yb[AlR_4]_2\}_n$ have been obtained according to a silylamide elimination reaction from $Yb[N(SiMe_3)_2]_2(THF)_2$ and excess AlR_3 (R = Me, Et, *i*Bu). While the tetramethylaluminate derivative is a pyrophoric powder which is insoluble in aliphatic and aromatic hydrocarbons, the ethyl and isobutyl congeners are readily soluble in *n*-hexane. Perethylated polymeric $\{Yb[AlEt_4]_2\}_n$ is constituted formally of the two molecular fragments $[Yb(AlEt_4)]^+$ and $[Yb(AlEt_4)_3]^-$, forming an intricate three-dimensional network in the solid state. Both fragments are linked by bridging α-carbon atoms and secondary Yb···H−C agostic interactions combining μ,η^1, μ,η^2, and μ,η^3 coordination modes which result in remarkably short Yb···Al (2.809(2) Å) and a large range of Yb···C (2.649(5)−3.364(6) Å) distances. DFT calculations on the molecular fragments $[Yb(AlEt_4)_3]^-$ and $[Yb(AlEt_4)]^+$ reproduced the X-ray geometry remarkably well. Moreover, the theoretical investigations on model systems for the aluminate coordination support the highly fluxional nature of the aluminate coordination ($\Delta E(\eta^2 \rightarrow \eta^3) = -8$ kcal/mol), which is also indicated by solution NMR spectroscopy. A topological analysis of the total electron density of the μ,η^2-bonded aluminate ligand in the benchmark systems $Y(AlR_4)_3$ (R = Me, Et) revealed the presence of two bond critical points between the Y−C_b and C_b−Al bonds (C_b = bridging carbon atom) and thus suggests a hypervalent character of the bridging carbon atom.

Downloaded by CARLI CONSORTIUM on June 29, 2009
Published on August 18, 2001 on http://pubs.acs.org | doi: 10.1021/om0102091

Introduction

Alkylaluminum reagents have been widely used to tailor the reactivity of early-transition-metal complexes in organic synthesis and olefin polymerization.[1] Prominent examples are the Tebbe reagent, $Cp_2Ti(\mu\text{-}CH_2)(\mu\text{-}Cl)AlMe_2$,[2] and lanthanidocene complexes of the type $Cp_2Ln(\mu\text{-}CH_3)_2Al(CH_3)_2$,[3] featuring preorganized heterobimetallic moieties. The $\eta^1 \rightarrow \eta^2 \rightarrow \eta^3$ fluxional behavior of the aluminate ligand and the presence of M···(CH) agostic interactions[4,5] are anticipated to significantly affect the reactivity of the latter complexes as well as to reveal mechanistic details of Ziegler−Natta polymerization processes.[6−8] Aside from the routinely observed μ,η^2-coordination mode, e.g., in $Cp_2Yb(\mu\text{-}CH_3)_2Al(CH_3)_2$,[3b] $[\mu,\eta^1]_2$, μ,η^1, and μ,η^3 bonding patterns were detected in $Cp^*_2Ln[\mu\text{-}CH_3Al(CH_3)_2(\mu\text{-}CH_3)]_2LnCp^*_2$ (Ln = Yb, Sm),[3e,9] $Cp^*_2Yb(\mu\text{-}C_2H_5)Al(C_2H_5)_2(THF)$,[10] and $[Al_3Nd_6(\mu\text{-}Cl)_6(\mu_3\text{-}Cl)_6(\mu\text{-}C_2H_5)_9(C_2H_5)_5(OiPr)]_2$.[11] The only structurally characterized homoleptic aluminate complexes comprise *polymeric* $[M(AlR_4)]_n$ (M = Li, Na, Rb, Cs)[12] and *monomeric* $Mg(AlMe_4)_2$[13] and $Ln(AlMe_4)_3$ (Ln

(1) Eisch, J. J. In *Comprehensive Organometallic Chemistry II*; Wilkinson, G., Stone, F. G. A., Abel, E. W., Eds.; Pergamon Press: Oxford, U.K., 1995; Volume 11, Chapter 6.

(2) Tebbe, F. N.; Parshall, G. W.; Reddy, G. S. *J. Am. Chem. Soc.* **1978**, *100*, 3611−3613.

(3) (a) Ballard, D. G. H.; Pearce, R. *J. Chem. Soc., Chem. Commun.* **1975**, 621. (b) Holton, J.; Lappert, M. F.; Ballard, D. G. H.; Pearce, R.; Atwood, J. L.; Hunter, W. E. *J. Chem. Soc., Dalton Trans.* **1979**, 45−53. (c) Scollary, G. R. *Aust. J. Chem.* **1978**, *31*, 411−414. (d) den Haan, K. H.; Wielstra, Y.; Eshuis, J. J. W.; Teuben, J. H. *J. Organomet. Chem.* **1987**, *323*, 181−192. (e) Busch, M. A.; Harlow, R.; Watson, P. L. *Inorg. Chim. Acta* **1987**, *140*, 15−20.

(4) (a) Evans, W. J.; Anwander, R.; Ziller, J. W. *Organometallics* **1995**, *14*, 1107−1109. (b) Evans, W. J.; Anwander, R.; Ziller, J. W.; Khan, S. I. *Inorg. Chem.* **1995**, *34*, 5927−5930. (c) Evans, W. J.; Ansari, M. A.; Ziller, J. W.; Khan, S. I. *Inorg. Chem.* **1996**, *35*, 5435−5444. (d) Klooster, W. T.; Lu, R. S.; Anwander, R.; Evans, W. J.; Koetzle, T. F.; Bau, T. *Angew. Chem.* **1998**, *110*, 1326−1329; *Angew. Chem., Int. Ed. Engl.* **1998**, *37*, 1268−1270.

(5) Siedle, A. R.; Newmark, R. A.; Schroepfer, J. N.; Lyon, P. A. *Organometallics* **1991**, *10*, 400−404.

(6) (a) Ballard, D. G. H.; Courtis, A.; Holton, J.; McMeeking, J.; Pearce, R. *J. Chem. Soc., Chem. Commun.* **1978**, 994−995. (b) Yasuda, H.; Tamai, H. *Prog. Polym. Sci.* **1993**, *18*, 1097−1139.

(7) (a) Bochmann, M.; Lancaster, S. J. *Angew. Chem.* **1994**, *106*, 1715−1718; *Angew. Chem., Int. Ed. Engl.* **1994**, *33*, 1634−1637. (b) Bochmann, M.; Lancaster, S. J. *J. Organomet. Chem.* **1995**, *497*, 55−59. (c) Bochmann, M.; Lancaster, S. J.; Robinson, O. B. *J. Chem. Soc., Chem. Commun.* **1995**, 2081−2082. (d) Bochmann, M. *J. Chem. Soc., Dalton Trans.* **1996**, 255−270.

(8) Brintzinger, H.-H.; Fischer, D.; Mülhaupt, R.; Rieger, B.; Waymouth, R. M. *Angew. Chem.* **1995**, *107*, 1255−1283; *Angew. Chem., Int. Ed. Engl.* **1995**, *34*, 1143−1170.

(9) (a) Evans, W. J.; Chamberlain, L. R.; Ulibarri, T. A.; Ziller, J. W. *J. Am. Chem. Soc.* **1987**, *109*, 7209−7211. (b) Evans, W. J.; Chamberlain, L. R.; Ziller, J. W. *J. Am. Chem. Soc.* **1988**, *110*, 6423−6432. (c) Evans, W. J.; Forrestal, K. J.; Ansari, M. A.; Ziller, J. W. *J. Am. Chem. Soc.* **1998**, *120*, 2180−2181.

(10) Yamamoto, H.; Yasuda, H.; Yokota, K.; Nakamura, A.; Kai, Y.; Kasai, N. *Chem. Lett.* **1988**, 1963−1966.

(11) Shan, C.; Lin, Y.; Quyang, J.; Fan, Y.; Yang, G. *Macromol. Chem.* **1987**, *188*, 629−635.

(12) For reviews, see: (a) Schade, C.; Schleyer, P. v. R. *Adv. Organomet. Chem.* **1987**, *27*, 169−278. (b) Weiss, E. *Angew. Chem.* **1993**, *105*, 1565−1587; *Angew. Chem., Int. Ed. Engl.* **1993**, *32*, 1501−1523.

(13) Atwood, J. L.; Stucky, G. D. *J. Am. Chem. Soc.* **1969**, *91*, 2538−2543.

10.1021/om0102091 CCC: $20.00 © 2001 American Chemical Society
Publication on Web 08/18/2001

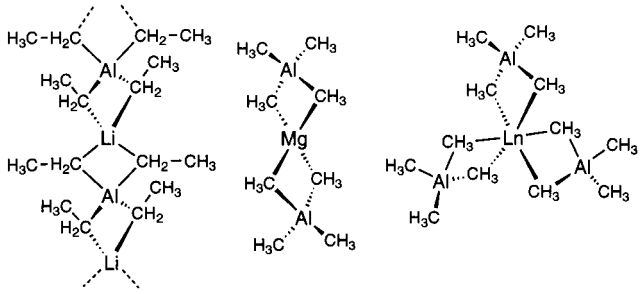

Figure 1. Structurally characterized homoleptic metal aluminate complexes.

= Y, Sm, Nd), which display the μ,η^2-coordination mode (Figure 1).[4]

Metal aluminate moieties can be generated by various synthetic routes, including addition of trialkylaluminum reagents to metal alkyl complexes, often termed AlR_3-mediated solvolysis (eq 1),[5,10,12−14] salt metathesis reactions involving metal halides (eq 2),[3] reduction of trialkylaluminum compounds (eq 3),[1,9,15] and amide elimination (eq 4).[4,16,17] Here, we describe the synthesis

$$Cp^*_2Yb(THF) + Al(C_2H_5)_3 \rightarrow Cp^*_2Yb(\mu\text{-}C_2H_5)Al(C_2H_5)_2(THF) \quad (1)$$

$$[Cp_2Yb(\mu\text{-}Cl)]_2 + 2LiAl(CH_3)_4 \rightarrow 2Cp_2Yb[Al(CH_3)_4] + 2LiCl \quad (2)$$

$$3Cp^*_2Sm(THF)_2 + 4Al(CH_3)_3 \rightarrow 3\{Cp^*_2Sm[Al(CH_3)_4]\} + Al \quad (3)$$

$$Ln(NMe_2)_3(LiCl)_3 + 6Al(CH_3)_3 \rightarrow Ln[Al(CH_3)_4]_3 + 1.5[Me_2Al(\mu\text{-}NMe_2)]_2 + 3LiCl \quad (4)$$

of the first polymeric transition-metal aluminate complexes via a silylamide elimination reaction. An X-ray crystallographic study on $\{Yb[AlEt_4]_2\}_n$ combined with a detailed theoretical treatment give new insights into the intrinsic versatility of aluminate coordination.

Results and Discussion

We found that the silylamide route[18] gives easy access to peralkylated Yb(II) aluminate complexes. $Yb[N(SiMe_3)_2]_2(THF)_2$ (**1**) reacts in *n*-hexane with an excess of the trialkylaluminum reagent to form the peralkylated heterobimetallic complexes **2**−**4** with a net composition of $\{Yb[AlR_4]_2\}$ (R = Me, Et, *i*Bu) (Scheme 1).[19,20]

Scheme 1. Synthesis of Homoleptic Yb(II) Aluminates via Silylamide Elimination (2, R = Me; 3, R = Et; 4, R = *i*Bu)

$$\underset{\mathbf{1}}{Yb[N(SiMe_3)_2]_2(THF)_2} + 6\,AlR_3 \xrightarrow[\text{r.t., 16 h}]{n\text{-hexane}} \underset{\mathbf{2\text{-}4}}{[Yb(AlR_4)_2]_n} + 2\{Al[N(SiMe_3)_2]R_2\} + 2\,AlR_3(THF)$$

The methyl derivative **2** precipitated quantitatively in analytically pure form as a yellow powder from the reaction mixture. Material **2** is insoluble in aliphatic and aromatic hydrocarbons and decomposes in tetrahydrofuran. In contrast, $\{Yb(AlEt_4)_2\}$ (**3**) and $\{Yb(Al\textit{i}Bu_4)_2\}$ (**4**) display excellent solubility in *n*-hexane and can easily be separated from the byproduct $\{Al[\mu\text{-}N(SiMe_3)_2]R_2\}$ as yellow well-shaped crystals via fractional crystallization at −35 °C. Their ^1H and ^{13}C NMR spectra revealed complete elimination of the silylamide ligands as well as the appearance of the ethyl and isobutyl signals, respectively, in correct integral ratios. A variable-temperature ^1H NMR study is consistent with a highly fluxional behavior of the terminal and bridging alkyl ligands: no decoalescence of the proton signals into separate resonances for the two types of alkyl groups could be resolved in the temperature range of −100 to +90 °C; interestingly, for the ethyl derivative, the methylene (δ ∼−0.06 ppm) and methyl signals (δ ∼1.34 ppm) broadened at −30 °C to reappear at −90 °C as slightly shifted sharp signals (−0.04 and 1.44 ppm, respectively).

1. Crystal Structure of 3. The solid-state structure of compound **3** was investigated by X-ray diffraction. The three-dimensional polymeric network formed by the Yb(II) cations and $AlEt_4^-$ anions constitutes formally of two molecular fragments (Figures 2a and 3a) $[Yb(AlEt_4)_3]^-$ and $[Yb(AlEt_4)]^+$. However, in the following, a more detailed structural investigation and theoretical model calculations will show that both fragments are linked by bridging α-carbon atoms and secondary Yb···H−C agostic interactions. Therefore, a simple structural description of **3** by a contact ion pair model is misleading.

(i) $[Yb(AlEt_4)_3]^-$ Fragment. The $[Yb(AlEt_4)_3]^-$ portion features a formally six-coordinated ytterbium center in a distorted-trigonal-antiprismatic geometry (Figure 2a) and conforms closely to C_3 symmetry. A similar overall coordination geometry was recently detected in homoleptic methylaluminate complexes of trivalent yttrium and neodymium.[4] In **3**, the μ,η^2-bridging ethyl moieties form large Yb(2)−C−C angles of 169° (average) comparable to the Li−C−C angle in $LiAlEt_4$ (174°)[21] and to the Sm−C−C angle in $Cp^*_2Sm(\mu\text{-}C_2H_5)_2Al(C_2H_5)_2$

Downloaded by CARLI CONSORTIUM on June 29, 2009
Published on August 18, 2001 on http://pubs.acs.org | doi: 10.1021/om0102091

(14) Tanner, P. S.; Williams, R. A.; Hanusa, T. P. *Inorg. Chem.* **1993**, *32*, 2234−2235.
(15) (a) Zakharkin, L. I.; Gavrilenko, V. V. *J. Gen. Chem. USSR (Engl. Transl.)* **1962**, *32*, 688−690. (b) Wolfrum, R.; Sauermann, G.; Weiss, E. *J. Organomet. Chem.* **1969**, *18*, 27−47. (c) Hoberg, H.; Krause, S. *Angew. Chem.* **1978**, *90*, 1013−1014; *Angew. Chem., Int. Ed. Engl.* **1978**, *17*, 949−950.
(16) (a) Her, T.-Y.; Chang, C.-C.; Liu, L.-K. *Inorg. Chem.* **1992**, *31*, 2291−2294. (b) Her, T.-Y.; Chang, C.-C.; Lee, G.-H.; Peng, S.-M.; Wang, Y. *Inorg. Chem.* **1994**, *33*, 99−104. (c) Chang, C.-C.; Lee, W.-H.; Her, T.-Y.; Lee, G.-H.; Peng, S.-M.; Wang, Y. *J. Chem. Soc., Dalton Trans.* **1994**, 315−322.
(17) Niemeyer, M.; Power, P. P. *Chem. Commun.* **1996**, 1573−1574.
(18) Anwander, R. *Top. Organomet. Chem.* **1999**, *2*, 1−61.
(19) Routinely employed Ln(III) tris(silylamide) complexes undergo such a silylamide elimination in the presence of the smaller ligand $N(SiHMe_2)_2$ only: Anwander, R.; Runte, O.; Eppinger, J.; Gerstberger, G.; Herdtweck, E.; Spiegler, M. *J. Chem. Soc., Dalton Trans.* **1998**, 847−858.
(20) The initially formed Lewis acid base adducts $Yb[N(SiMe_3)_2]_2(AlR_3)_2$ (R = Me, Et) were previously isolated, the methyl derivative was structurally characterized, and their activity in ethylene polymerization (20 °C, 12 atm) was revealed: Boncella, J. M.; Andersen, R. A. *Organometallics* **1985**, *4*, 205−206.
(21) Gerteis, R. L.; Dickerson, R. E.; Brown, T. L. *Inorg. Chem.* **1964**, *3*, 872−875.

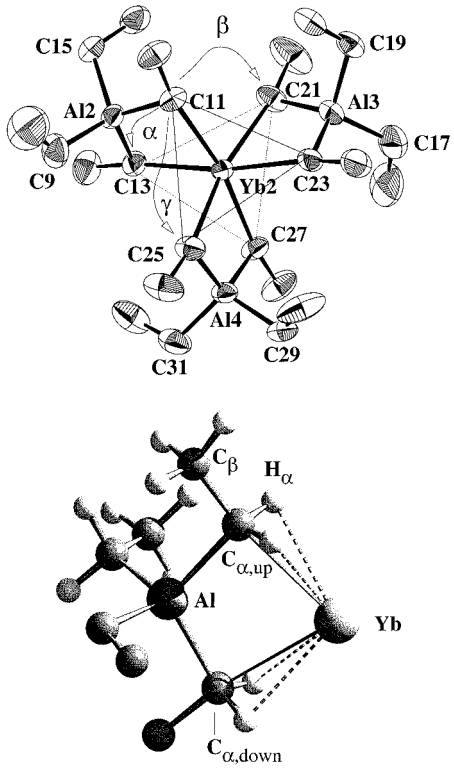

Figure 2. (a, top) PLATON[54] drawing of the anionic fragment $[Yb(AlEt_4)_3]^-$ of the 3-dimensional network. (b, bottom) SCHAKAL[55] drawing of the corresponding DFT model system $[Yb(AlEt_4)_3]^-$ at the BPW91/I level of theory. Only one $AlEt_4^-$ ligand is shown (C_3 symmetry). Atoms of the experimental study are represented by thermal ellipsoids at the 50% probability level. The $[Yb(AlEt_4)_3]^-$ anion in the solid state closely conforms to C_3 symmetry. Assuming ideal C_3 symmetry, the C_α atoms can be classified into two symmetry-related groups: C11, C23, C25 (C_{up}) and C13, C21, C27 (C_{down}). As shown in (a), the atoms C_{up} atoms lie above a plane which is defined to be orthogonal with respect to the C_3 axis and contains the ytterbium atom (atoms labeled (′) belong to terminal ethyl groups). Selected bond lengths (Å) and angles (deg) (calculated values are shown in brackets): Yb2···C_α = 2.649(5)−2.700(7) [2.755−2.767], Yb2···Al = 3.1884(17)−3.2180(17) [3.309], [Yb···H_α = 2.562−2.610], Al−C_α = 2.045(7)−2.071(5) [2.109−2.112], Al−C_α' = 1.985(8)−2.033(6) [2.034−2.035]; C_{up}−Yb−C_{up} = 93.5 (av) [91.8], C_{down}−Yb−C_{down} = 94.0 (av) [93.2], α(C_{up}−Yb−C_{down}) = 78.7(2)-79.8(2) [78.8], β(C_{up}−Yb−C_{down}) = 93.8(2)−94.0(2) [97.5], γ(C_{up}−Yb−C_{down}) = 169.4(2)−171.1(2) [166.92], C_α−Al−C_α = 112.0(2)−112.4(2) [112.3], Yb2−C_α−C_β = 167.7(5)−170.2(5) [169.8−170.4].

(170(4)°).[9a] The average Yb^{II}(2)−C(CH_2) bond length of 2.675 Å is similar to that of 2.61(2) Å found in eight-coordinated $Cp_2Yb^{III}(\mu\text{-}CH_3)_2Al(CH_3)_2$,[3b] taking into account the different coordination numbers and oxidation states.[22] For comparison, as expected, the Yb^{II}−C σ-bond distances in homoleptic $Yb^{II}[C(SiMe_3)_3]_2$ (average 2.495 Å)[23a,c] and heteroleptic $Yb^{II}(C_6H_3Ph_2\text{-}2,6)I(THF)_3$ (2.529(4) Å) are considerably shorter.[23b]

DFT calculations at the BPW91/I level of theory on the molecular $[Yb(AlEt_4)_3]^-$ fragment reproduced the X-ray geometry remarkably well. In Figure 2b the fully optimized $[Yb(AlEt_4)_3]^-$ geometry with C_3 symmetry restraint is shown. We note that the calculated average Yb···Al and Yb−C bond distances of 3.309 and 2.761 Å, respectively, are slightly larger compared with the experimental values (3.200 and 2.675 Å). This is possibly due to intermolecular interactions and charge transfer between the formal $[Yb(AlEt_4)_3]^-$ and $[Yb(AlEt_4)]^+$ fragments. While the positions of the hydrogen atoms could not be precisely determined by X-ray diffraction, the agostic character of the α-hydrogen atoms is clearly revealed in the DFT calculation on the model system. The average Yb···C−H valence angles of 69.3° and the Yb···H bond distances of 2.586 Å are remarkably small. However, the corresponding average C_α−H bond distances of 1.115 Å are only slightly enlarged compared with the nonagostic C_β−H bonds of the bridging ethyl groups (about 1.104 Å; averaged value). Thus, no significant C−H activation can be established on the basis of the geometrical parameters. We note that the valence angles and the short Yb−C bonds suggest a hypervalent character of the bridging carbon atom: ∠Al−C−Yb = 84.45°; ∠Al−C_α−C_β = 105.3°; ∠Al−C_α−H_α = 116.7°; averaged values. The nature of this special type of agostic interaction will be discussed in greater detail on the basis of a topological analysis in a subsequent section.

(ii) $[Yb(AlEt_4)]^+$ Fragment. As shown in Figure 3a, the $[Yb(AlEt_4)]^+$ fragment displays a rare μ,η^3-coordination mode of the aluminate ligand. The average Yb(1)−C−C angle within the μ,η^3-bonded aluminate is found to be approximately 120°, which differs markedly from that observed in the μ,η^2-bonded moieties (169°). In addition, the μ,η^3 aluminate coordination causes an extremely short Yb(1)···Al contact of 2.809(2) Å, which compares well with the corresponding average Nd···Al distance of 2.83 Å originally observed in $[Al_3Nd_6(\mu\text{-}Cl)_6$-

(22) The ionic radius in Yb^{II} is 0.15 Å larger compared with the corresponding radius for Yb^{III}: Shannon, R. D. *Acta Crystallogr.* **1976**, *A32*, 751−767.

(23) (a) Eaborn, C.; Hitchcock, P. B.; Izod, K.; Smith, J. D. *J. Am. Chem. Soc.* **1994**, *116*, 12071−12072. (b) Heckmann, G.; Niemeyer, M. *J. Am. Chem. Soc.* **2000**, *122*, 4227−4228. (c) We note that the standard Yb^{II}−C single-bond length and the assumed difference between the ionic radii of Yb^{II} and Yb^{III} centers are confirmed by the DFT calculations at the BPW91/I level of theory on the model systems $YbMe_2$ and $YbMe_3$: Yb^{II}−C = 2.48 Å and Yb^{III}−C = 2.34 Å. The calculated values compare reasonably well with the averaged experimental values of 2.495 Å in $Yb^{II}[C(SiMe_3)_3]_2$[23a] and 2.379 Å in $Yb^{III}(CH_2tBu)_3(THF)_2$ (Niemeyer, M. *Z. Anorg. Allg. Chem.* **2000**, *626*, 1027−1029) for the averaged Yb^{II}−C and Yb^{III}−C bond distances, respectively, thus justifying the chosen method of calculation. We note that the calculated *bent* ($YbMe_2$; ∠C−Yb^{II}−C = 108.8°) and *pyramidal* ($YbMe_3$; ∠C−Yb^{III}−C = 107.7°) structures can be rationalized by taking into account the nonideally spherical shape of the valence shell of the Yb atom. The distortion produced by the ligands results in *four* local charge concentrations (as shown by a topological analysis of the Laplacian of the electron density) in a tetrahedral arrangement around the Yb atom. The mutual repulsion between these charge concentrations and the ligands leads to a *bent* structure of the divalent ytterbium compounds, such as in $YbMe_2$. Similar geometrical preferences have been previously found in difluorides and dihydrides of group 2 metal compounds (Bytheway, I.; Gillespie, R. J.; Tang, T.-H.; Bader, R. F. W. *Inorg. Chem.* **1995**, *34*, 2407−2414). It seems, therefore, quite plausible to resort to the same arguments to explain the experimentally observed bent structure of $Yb(C_5Me_5)_2$ (∠C_g1−Yb−C_g2 = 156°, where C_g stands for a ring centroid) (Andersen, R. A.; Boncella, J. M.; Burns, C. J.; Blom, R.; Haaland. A.; Volden, H. V. *J. Organomet. Chem.* **1986**, *312*, C49). The same explanation can be found elsewhere (Bytheway, I.; Popelier, P. L. A.; Gillespie, R. J. *Can. J. Chem.* **1996**, *74*, 1059−1071). We should also note that the results obtained from a topological analysis of the Laplacian of the electron density based on the use of an effective core potential (ECP) for modeling core electrons of the metal center have been shown to be *qualitatively* the same, with respect to the number and arrangement of the local charge concentrations, as those obtained from all-electron calculations (see: Sierraalta, A.; Ruette, F. *Int. J. Quantum Chem.* **1996**, *60*, 1015−1026). The main effect of employing the ECP in the calculations is the *shortening* of the distances from a metal center to the local charge concentrations as compared to those from all-electron calculations.

Downloaded by CARLI CONSORTIUM on June 29, 2009
Published on August 18, 2001 on http://pubs.acs.org | doi: 10.1021/om0102091

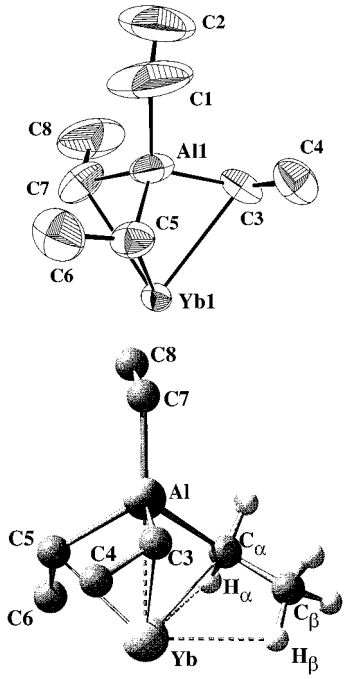

Figure 3. (a, top) PLATON[54] drawing of the cationic fragment $[Yb(AlEt_4)]^+$ of the three-dimensional network. (b, bottom) SCHAKAL[55] drawing of the corresponding DFT model system $[Yb(AlEt_4)]^+$ at the BPW91/I level of theory. Atoms of the experimental study are represented by thermal ellipsoids at the 50% probability level (atoms labeled (′) belong to terminal ethyl groups). Selected bond lengths (Å) and angles (deg) (calculated values are shown in brackets): Yb···Al = 2.809(2) [2.696], Yb−C_α = 2.744(6)−2.824(5) [2.573−2.575], Al1−C_α = 2.016(8)−2.076(12) [2.136−2.140], Al1−C_α' = 2.001(15) [1.978], [Yb···C_β = 2.940−2.952, Yb···H_α = 2.698−2.716, Yb···H_β = 2.493−2.507, C_α−H_α = 1.115, C_β−H_β = 1.124], C_α−Yb−C_α = 71.5(3)−72.3(2) [79.8−80.0]; Al1−C_α−C_β = 108.3(7)−113.7(8) [124.5−125.1], Al1−C_α'−C_β' = 123.6(14) [115.9], [C_α−C_β−H_β = 115.8−115.9, Al−C_α−H_α = 116.3−116.6, Yb−C_α−H_α = 84.1−85.1], Yb2−C_α−C_β = 115.5(6)−123.4(5) [87.3−87.7].

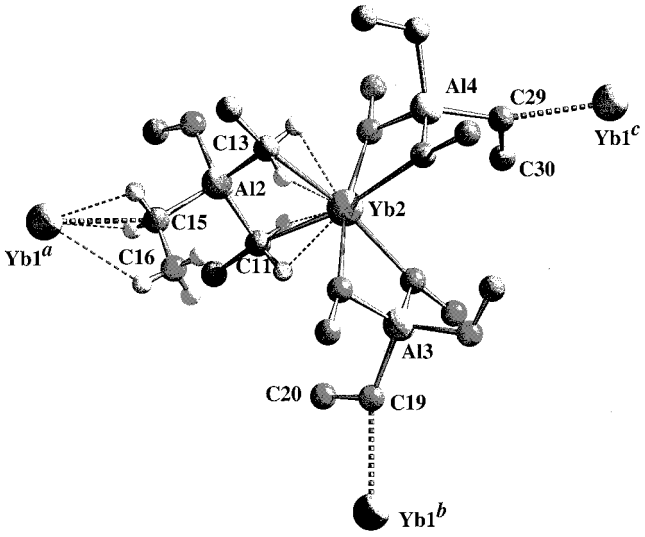

Figure 4. Fragment of the three-dimensional network of **3**, showing the linkage between the $[Yb2(AlEt_4)_3]^-$ and three $[Yb1(AlEt_4)]^+$ fragments by bridging Yb···C_{CH_2} contacts and Yb1···H−C secondary interactions, resulting in a $\mu,\eta^2/\mu,\eta^1$ coordination mode. For clarity only selected H atom positions are shown. Symmetry operations: (a) $1 + x, y, z$; (b) $2 - y, 2 + x - y, -^1/_3 + z$; (c) $-x + y, 2 - x, ^1/_3 + z$. Salient bond lengths (Å) and angles (deg): Yb1^a···C15 = 2.818(5), Yb1^b···C19 = 2.795(6), Yb1^c···C29 = 2.778(6), C15−C16 = 1.516(10), C19−C20 = 1.528(8), C29−C30 = 1.523(10); Al2−C15−C16 = 114.4(4), Al3−C19−C20 = 115.2(4), Al4−C29−C30 = 116.2(5), Yb1^a···C15−C16 = 97.3(3), Yb1^b···C19−C20 = 90.0(4), Yb1^c···C29−C30 = 85.3(4).

$(\mu_3\text{-Cl})_6(\mu\text{-}C_2H_5)_9(C_2H_5)_5(O\textit{i}Pr)]_2$.[11] In the μ,η^2-bonded aluminate moieties a significantly larger average Yb(2)···Al distance of 3.20 Å is observed instead. DFT calculations at the BPW91/I level on the model system $[Yb(AlEt_4)]^+$, however, indicate even shorter Yb···Al distances of 2.70 Å and suggest a significant compensation of the positive charge at the Yb center in the solid state (Figure 3b). Indeed, in the next section we will show that the $[Yb(AlEt_4)]^+$ fragment is coordinated by six carbon atoms and shielded by further secondary interactions.

(iii) Linkage of the $[Yb(AlEt_4)_3]^-$ and $[Yb(AlEt_4)]^+$ Fragments. Figure 4 reveals that in the solid state *each one* of the three μ,η^2-bonding aluminate ligands forms *one* linkage between the $[Yb2(AlEt_4)_3]^-$ and a $[Yb1(AlEt_4)]^+$ fragment by bridging Yb···C_{CH_2} contacts and Yb1···H−C secondary interactions, resulting in an unprecedented $\mu,\eta^2/\mu,\eta^1$-coordination mode. These μ,η^1-bridging ethyl groups approach the Yb(1) centers side-on, forming additional close Yb···C_{CH_3} contacts in the range 3.056(9)−3.364(6) Å. As a consequence, the Yb−C_{CH_2}−C_{CH_3} connections involved exhibit rather acute angles of 85.3(4)−97.3(3)° which are indicative of pronounced agostic deformations.[24,25] We note that the position of the hydrogen atoms could be located and suggest the presence of *two* α- and *one* β-agostic Yb1···H coordination modes formed by the side-on-coordinated ethyl groups. A similar side-on bonding situation was previously found in $Cp^*_2Yb(\mu\text{-}C_2H_5)Al(C_2H_5)_2(THF)$ (Yb−C, 2.854(18) and 2.939(21) Å; ∠Yb−C−C 76.6°).[10,26] However, the aluminate bonding situation in this compound is slightly different, since the $Al(C_2H_5)_3$ ligand forms an adduct with the Cp^*_2Yb unit. The agostic interactions were described as being negligible, since for the bridging ethyl group a rather large C−C bond distance of 1.63(3) Å was found in contrast to the common experience that "the agostic interaction generally brings about the shortening of the ethyl C−C bond (by 0.06−0.08 Å)".[27] However, in **3** C−C bond distances for the agostic μ,η^1-bridging ethyl groups in the small range 1.516(10)−1.528(8) Å were observed instead. These distances compare well with the ethyl C−C bond distance of 1.512(1) Å observed in a precise experimental charge density study on the β-agostic $EtTiCl_3(dmpe)$ (dmpe = 1,2-bis(dimethylphosphino)-ethane).[28]

(24) Burger, B. J.; Thompson, M. E.; Cotter, W. D.; Bercaw, J. E. *J. Am. Chem. Soc.* **1990**, *112*, 1566−1577.

(25) (a) Brookhart, M.; Green, M. L. H. *J. Organomet. Chem.* **1983**, *250*, 395−408. (b) Haaland, A.; Scherer, W.; Ruud, K.; McGrady, G. S.; Downs, A. J.; Swang, O. *J. Am. Chem. Soc.* **1998**, *120*, 3762−3772 and references therein.

(26) μ,η^1-Bridging ethyl groups are routinely observed in alkali-metal chemistry: e.g., in $K[Al_2Et_6F]$. See: (a) Natta, G.; Allegra, G.; Perego, G.; Zambelli, A. *J. Am. Chem. Soc.* **1961**, *83*, 5033. (b) Allegra, G.; Perego, G. *Acta Crystallogr.* **1963**, *16*, 185−190.

(27) Unfortunately, the position of the potential agostic hydrogen atoms in $Cp^*_2Yb(\mu\text{-}C_2H_5)Al(C_2H_5)_2(THF)$ could not be located.

Downloaded by CARLI CONSORTIUM on June 29, 2009
Published on August 18, 2001 on http://pubs.acs.org | doi: 10.1021/om0102091

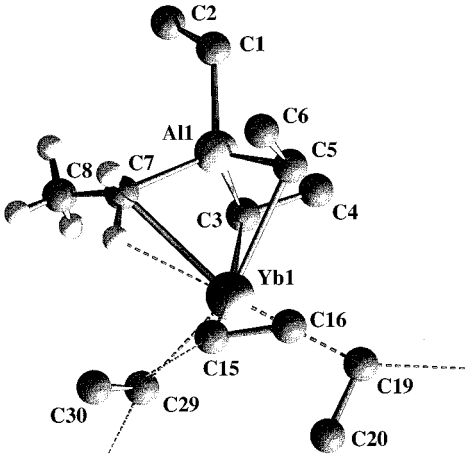

Figure 5. Fragment of the three-dimensional network of **3**, showing the coordination sphere of the Yb1 center which is completed by *three* side-on coordinated ethyl groups, resulting in a total coordination number of 6. For clarity only selected H atom positions of one ethyl group from the μ,η^3-coordinated aluminate ligand are shown. See also Figures 2a, 3a, and 4 for further information and definition of geometrical parameters and the classification of ligating atoms (C_{up} = C3, C5, C7; C_{down} = C15, C19, C29). Salient angles (deg): $C_{up}-Yb1-C_{up}$ = 71.9 (av), $C_{down}-Yb1-C_{down}$ = 100.4 (av), C3−Yb1−C15 = 163.4(2), C3−Yb1−C19 = 91.1(2), C3−Yb1−C29 = 87.0(2).

Figure 5 shows that the coordination sphere of the Yb1 center is completed by *three* side-on-coordinated ethyl groups, resulting in a total coordination number of 6. Surprisingly, the Yb(1)−C bond lengths of the η^3-coordinated aluminate ligand and that of the μ,η^1-bridging ethyl moieties fall in the narrow range of 2.744(6)−2.824(5) Å and are only slightly larger compared with the corresponding average Yb(2)−C bond distances of 2.675 Å of the μ,η^2-coordinated aluminate ligands.

Figure 5 finally displays a third type of agostic interaction present in **3** involving three α-C_{CH_2}−H bonds of the μ,η^3-coordinated aluminate ligand. Taking into account that the Yb1 center is now efficiently shielded by 12 Yb···H−C secondary interactions (9 α-agostic and 3 β-agostic interactions), we assume that the effective charge at both Yb centers should be comparable, despite the fact that in $[Yb(AlEt_4)_3]^-$ slightly shorter Yb−C bond distances are observed than in $[Yb(AlEt_4)]^+$. This results stresses again the polymeric character of **3**, ruling out a simple description of **3** by an ion pair model.

The importance of secondary interactions to complete the coordination spheres of the large Yb^{II} metal centers is also demonstrated by the result of the DFT optimizations on the hypothetical $[Yb(AlEt_4)]^+$ fragment. Here the increased charge deficiency of the sterically less shielded metal center is compensated (Figure 3b) by even shorter Yb···C_α and Yb···C_β distances (2.573−2.575 and 2.940−2.952 Å, respectively) and by additional α- and β-agostic interactions (Yb···H_α = 2.698−2.716 Å, Yb···H_β = 2.493−2.507 Å). This example also reinforces the unusual coordination flexibility of the aluminate ligand.

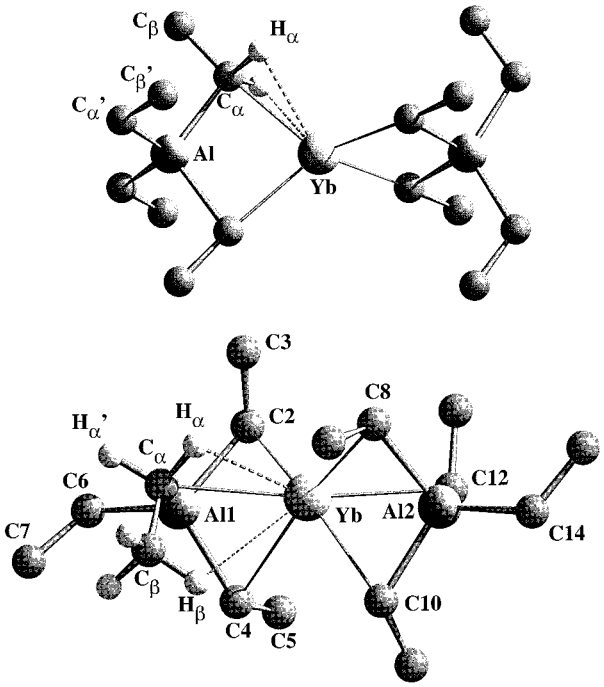

Figure 6. $Yb[AlEt_4]_2$ model systems: (a, top) $\mu,\eta^2/\mu,\eta^2$-bridging mode, (b, bottom) $\mu,\eta^3/\mu,\eta^3$-bridging mode (C_{up} = C_α, C2, C4; C_{down} = C8, C10, C12). Important bond lengths (Å) and angles (deg): (a) Yb···C_α = 2.592, Yb···H_α = 2.488, Yb···Al = 3.109, $C_\alpha-C_\beta$ = 1.549, $C_\alpha'-C_\beta'$ = 1.545, $C_\alpha-H_\alpha$ = 1.122, $C_\beta-H_\beta$ = 1.102−1.105, $C_\alpha-Yb-C_\alpha$ = 86.3, $C_\alpha-Al-C_\alpha$ = 111.0, $Al-C_\alpha-Yb$ = 81.3, $Yb-C_\alpha-C_\beta$ = 174.9, $Al-C_\alpha-C_\beta$ = 103.8; (b) Yb···Al = 2.856−2.863, Yb···C = 2.769−2.890, Yb···C_α =2.806, $C_\alpha-C_\beta$ = 1.548, C6−C7 = 1.544, $C_\alpha-H_\alpha$ = 1.119, $C_\alpha-H_\alpha'$ = 1.108, $C_\beta-H_\beta$ = 1.109, $C_\beta-H_\beta'$ = 1.103−1.105, Yb···H_α = 2.565, Yb···H_β = 3.092, $C_{up}-Yb-C_{up}$ = 73.1 (av), $C_{down}-Yb-C_{down}$ = 72.7 (av), $C_\alpha-Yb-C8$ = 104.5, $C_\alpha-Yb-C10$ = 114.4, $C_\alpha-Yb-C12$ = 172.2, $Yb-C_\alpha-C_\beta$ = 102.1.

2. Structural Models for $Yb[AlEt_4]_2$. On the basis of the solution NMR data and solid-state structure of compound **3**, a rather flexible aluminate coordination is suggested, fluctuating between extremely reactive (because large) terminal Yb···C contacts in **I**, the commonly observed μ,η^2-bridging mode **II**, and an unusually coordinated aluminum center in **III** (Scheme 2).

To get a more detailed picture of the intrinsic nature of the aluminate bonding explorative DFT calculations at the BPW91/I level of theory were carried out for the three different kinds of homoleptic aluminate systems $Yb[AlEt_4]_2$: (i) $\mu,\eta^2/\mu,\eta^2$-bridging mode (**3a**), (ii) $\mu,\eta^2/\mu,\eta^3$-bridging mode (**3b**), and (iii) $\mu,\eta^3/\mu,\eta^3$-bridging mode (**3c**) (Figure 6). The optimizations on **3a** converged to a model with D_{2d} overall symmetry (Figure 6a). The bridging methylene groups in **3a** display remarkably short Yb···C and secondary Yb···H distances of 2.592 and 2.488 Å, respectively. Those distances are much shorter compared with the solid-state $\{Yb[AlEt_4]_2\}_n$ species and indicate an insufficient shielding of the Yb(II) center. This result is supported by analytical frequency calculations on **3a** showing two low imaginary

(28) The ethyl C−C bond distances of the nonbridging ethyl groups in **3** are shorter (1.414(15)−1.493(12) Å) in comparison with the μ,η^1-bridging ethyl groups. However, the shortening of these C−C bonds might also be caused by higher librational motion and/or some degree of disorder due to the higher structural flexibility of these noncoordinated ethyl groups. Unfortunately, we could not sort out this problem by a high-resolution low-temperature X-ray study, since all investigated crystals of **3** start to powderize at temperatures below −50 °C; see: Scherer, W.; Hieringer, W.; Spiegler, M.; Sirsch, P.; McGrady, G. S.; Downs, A. J.; Haaland, A.; Pedersen, B. *Chem. Commun.* **1998**, 2471−2472.

Downloaded by CARLI CONSORTIUM on June 29, 2009
Published on August 18, 2001 on http://pubs.acs.org | doi: 10.1021/om0102091

Scheme 2. Aluminate Coordination Mobility Detected in Rare-Earth Complexes

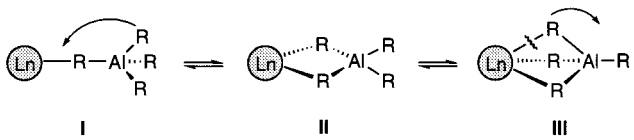

I II III

frequencies (∼17*i* cm^{-1}), which indicate that **3a** corresponds to a second-order saddle point on the potential energy surface (PES). Analysis of the modes of these imaginary frequencies suggest that distortions toward a $\mu,\eta^3/\mu,\eta^3$-bridging mode should lead to energetically favored geometries.

Indeed, at the BPW91/I level of theory the $\mu,\eta^3/\mu,\eta^3$-bridging mode appears to be the most stable conformation. However, even in the case of **3c**, vibrational analysis at the stationary point revealed two low imaginary frequencies of ∼4*i* and ∼23*i* cm^{-1} (second-order saddle point) that correspond to vibrations of the terminal and bridging ethyl groups, respectively. As shown in Figure 6b, our model system (C_1 symmetry) with the lowest energy on the BPW91/I PES displays six bridging methylene groups surrounding the ytterbium metal core in a distorted-antiprismatic fashion: $\tau(C_\alpha-Al1\cdots Al2-C12)$ = 158°. Due to the sterically favored antiprismatic coordination mode and the presence of two noncoordinating ethyl groups, no higher symmetric ligand arrangement seems to be reasonable. The local symmetry is further reduced by a bending of the Al···Yb···Al axis by 172°. We note that the Yb···C distances (2.769−2.890 Å) are now in the same range as for the μ,η^3-bridging aluminate ligand in the solid-state structure (2.744(6)−2.824(5) Å). These results suggest that the shielding of the Yb center in our best monomeric model for $Yb[AlEt_4]_2$ seems to be reasonable. We further note that the metal shielding in **3c** is also supported by six α-agostic and six *β*-agostic Yb···H interactions.

However, the energy differences between the three model systems are marginal (0.0, 4.2, and 8.3 kcal/mol for $\mu,\eta^3/\mu,\eta^3$, $\mu,\eta^2/\mu,\eta^3$, and $\mu,\eta^2/\mu,\eta^2$ bridging mode systems, respectively, without zero-point corrections), supporting the NMR results.[29] This is in accordance with the aforementioned experimental findings of variable-temperature NMR studies, which show only one broadened proton signal for bridging and terminal alkyl groups in **3** at −30 °C. Note that for the previously reported homoleptic $Ln(AlMe_4)_3$ (Ln = Y, Sm, Nd),[4] featuring the markedly smaller Ln(III) centers, separate resonances for the two types of methyl groups could be resolved as 1:1 signals at lower temperature for the smaller yttrium (−60 °C) and samarium (−80 °C). The neodymium derivative gave only a broadened signal at −80 °C.

3. Topological Analysis of Aluminate Coordination. (i) Nature of the Bonding in μ,η^2-Coordinated Aluminate Species. Despite the impressive variety of bonding modes in the $[AlEt_4]^-$ aluminate ligand coordination displayed in the solid-state structure of **3**, and the homoleptic model systems **3a**−**c** the standard μ,η^2-bonded coordination mode seems to dominate the coordination chemistry of sterically more demanding systems, such as the catalytically relevant species $Cp^*_2Sm[(\mu\text{-}C_2H_5)_2Al(C_2H_5)_2]$ and *rac*-$[Me_2Si(2\text{-}Me\text{-}C_9H_5)_2]Y[(\mu\text{-}C_2H_5)_2Al(C_2H_5)_2]$.[30] Unfortunately, due to the lack of accurate structural data the nature of the aluminate bonding and of Ln···H secondary interactions in these types of complexes remains unclear. The contribution of so-called "*polyagostic*" interactions was first proposed for the homoleptic species $[Nd(AlMe_4)_3]$ on the basis of a neutron diffraction study, which revealed acute Nd···C−H_α angles of 80.3(4)° associated with the bridging H atoms.[4a] Heteropolyagostic interactions have been discussed in $Nd[NiPr_2][(\mu\text{-}NiPr_2)(\mu\text{-}Me)AlMe_2][(\mu\text{-}Me)_2AlMe_2]$ on the basis of an X-ray diffraction study.[31] However, no activation of the bridging C_α−H bonds (C−H = 1.08(1) Å) relative to the terminal ones (C−H = 1.09(1) Å) was observed. To gain a better insight into the electronic structure of the μ,η^2-bonded aluminate ligands, a topological analysis of the total electron density using Bader's "atoms in molecules" (AIM) approach[32] was performed. We decided to study the theoretical charge density of the monomeric trivalent model systems $Y[AlR_4]_3$ (R = Me (**5**), Et (**6**)), since these (i) are neutral, (ii) possess a high symmetry (C_3), and (iii) display stable μ,η^2-coordination of the aluminate ligand, since the metal core is sufficiently shielded by three aluminate ligands in contrast to $Yb[AlEt_4]_2$.

(ii) Ln···C−Al Bonding Situation. Figure 7a shows the BPW91/II optimized core geometry of $Y[AlEt_4]_3$ (**6**), which is isostructural with the $Yb[AlEt_4]_3^-$ fragment of the solid-state structure of **3**. As shown in Table 1, the average Y−C bond distances of 2.57 Å are slightly longer compared with the corresponding values of the methyl analogue as obtained by experiment (Y−C = 2.508(7) Å) and calculations (Y−C = 2.55 Å). The calculations suggest a slight asymmetry of the C_3 symmetric core geometry: the six methylene groups form a slightly distorted antiprism with $C_{up}-Y-C_{up}$ = 90.7° and $C_{down}-Y-C_{down}$ = 91.4°. This distortion is also reflected in slightly different C_{up}−Y and C_{down}−Y distances of 2.580 and 2.569 Å, respectively (Table 1).[33] However, in the following we will ignore these minor distortions and refer to average values.

Figure 7b shows the contour map of the Laplacian of the electron density for $Y[\mu,\eta^2\text{-}AlEt_4]_3$ (**6**) projected into the $Y-C_{CH_2}-Al$ plane. The bond paths connecting both bridging C_b atoms with the Y and the Al metal centers clearly demonstrate the hypervalent character of the bridging C atoms (coordination number 5). Furthermore, all bond paths are curved inwards, confirming the

(29) Table S1 in the Supporting Information further indicates that the differences in chemical shifts for the μ,η^2- and μ,η^3-coordinated aluminate ligands in the ^1H and ^{13}C NMR spectra are rather small.

(30) Klimpel, M.; Anwander, R.; Scherer, W.; Sirsch, P.; Tafipolsky, M., unpublished results.

(31) Evans, W. J.; Anwander, R.; Ziller, J. N.; Khan, S. I. *Inorg. Chem.* **1995**, *34*, 5927−5930.

(32) (a) Bader, R. F. W. *Atoms in Molecules: A Quantum Theory*; Oxford University Press: Oxford, U.K., 1990; International Series of Monographs on Chemistry, Vol. 22. (b) Biegler-König, F. W.; Bader, R. F. W.; Tang, T. *J. Comput. Chem.* **1982**, *3*, 317−328.

(33) This result might be interesting for the comparison with the neutral *non*-VSEPR structures of the MMe_6 transition-metal complexes of Mo and W. In those C_3-symmetric complexes a strongly distorted prismatic ligand arrangement is observed with two sets of Me−M−Me angles and Me−M distances. See: (a) Haaland, A.; Hammel, A.; Rypdal, K.; Volden, H.-V. *J. Am. Chem. Soc.* **1990**, *112*, 4547−4549. (b) Kaupp, M. *Chem. Eur. J.* **1998**, *4*, 1678−1686. (c) Kleinhenz, S.; Pfennig, V.; Seppelt, K. *Chem. Eur. J.* **1998**, *4*, 1687−1691. (d) Roessler, B.; Seppelt, K. *Angew. Chem.* **2000**, *112*, 1326−1329; *Angew. Chem., Int. Ed.* **2000**, *39*, 1259−1261.

Downloaded by CARLI CONSORTIUM on June 29, 2009
Published on August 18, 2001 on http://pubs.acs.org | doi: 10.1021/om0102091

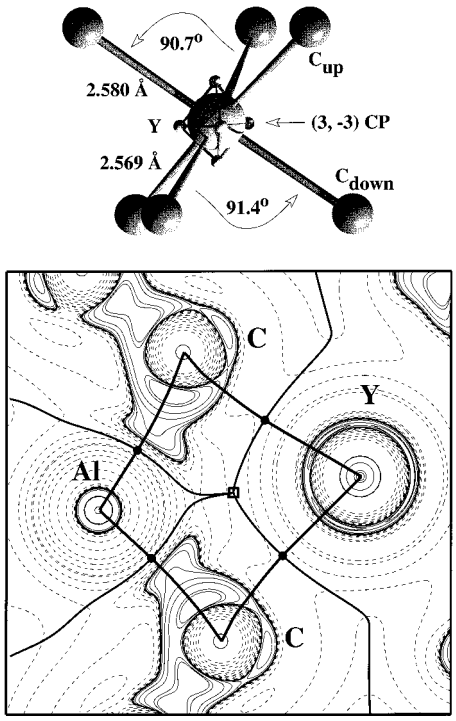

Figure 7. (a, top) Distorted antiprismatic core geometry of $Y[AlEt_4]_3$ (**6**) at the BPW91/II level of theory. Five charge concentrations as located by (3,−3) CPs in the Laplacian of $\rho(\mathbf{r})$ are shown as closed circles forming a trigonal bipyramid (tbp). The corresponding charge depletions, (3,+1) CPs, are located close to the midpoints of the six faces of the tbp formed by the five CCs. (b, bottom) Contour map of the Laplacian of $\rho(\mathbf{r})$ for **6** projected into the $Y-C(CH_3)-Al$ plane (contour levels are drawn at 0.001, $\pm 2.0 \times 10^n$, $\pm 4.0 \times 10^n$, $\pm 8.0 \times 10^n$ e Å^{-5}, where $n = 0$, -3, ± 2, ± 1; positive and negative values are marked by dashed and solid lines, respectively). An additional contour line at -9.5 e Å^{-5} is shown to clarify the polarization of the outer shell of the core of the Y atom. The atomic boundaries, as determined by the zero-flux surface condition, along with the bond paths in the electron density are also indicated. Bond CPs are denoted by closed circles; the ring CP is denoted by an open square.

electron-deficient character of the $[YC_2Al]$ fragments.[32] Surprisingly, the electron density at the Y···C bond critical points (CPs) is rather pronounced ($\rho(\mathbf{r}_c) = 0.24$ e Å^{-3}) and not significantly reduced in comparison with the corresponding C_b-Al bond CPs ($\rho(\mathbf{r}_c) = 0.38$ e Å^{-3}) (Table 1).

Thus, a simple description of the lanthanide aluminates as contact ion pairs Y^{3+}/AlR_4^- is not supported by analysis of the topology of the charge density. Indeed, in comparison with the nonbridging Al−C bonds ($\rho(\mathbf{r}_c) = 0.51$ e Å^{-3}) the bridging $Al-C_b$ bonds in **6** seem to be weakened at the expense of significant Y···C interactions. The weakening of the bridging $Al-C_b$ bonds ($Al-C_b = 2.14$ Å) is also indicated by an elongation of 0.13 Å relative to the nonbridging Al−C bonds (Al−C = 2.01 Å). The low value of $\rho(\mathbf{r}_c)$, the large $Al-C_b$ separation, and a positive value of the Laplacian ($\nabla^2\rho(\mathbf{r}_c) = 3.8$ e Å^{-5}) might indicate a purely closed-shell $Al-C_b$ bonding interaction (Table 1). However, analysis of both kinetic energy densities $G(\mathbf{r})$ and potential energy densities $V(\mathbf{r})$ at the bond CPs suggests some covalent character for the $Al-C_b$ bonds: $H(\mathbf{r}_c) = G(\mathbf{r}_c) + V(\mathbf{r}_c) = -0.11$ hartree Å^{-3}; $G(\mathbf{r}_c)/\rho(\mathbf{r}_c) = 0.98$ hartree e^{-1}. We conclude that

Table 1. Topological Parameters for the Charge Density of the $Y[AlMe_4]_3$ and $Y[AlEt_4]_3$ Model Systems at the BPW91/II Level[a,b]

	Y−C$_b$	Al−C$_b$	Al−C$_t$	C$_b$−C$_{Me}$	C$_t$−C$_{Me}$	ring
			$Y[AlMe_4]_3$			
r(A−B)						
exptl[c]	2.51	2.08	1.96			
calcd	2.55	2.13	1.99			
$\rho(\mathbf{r}_c)$	0.28	0.37	0.53			0.16
$\nabla^2\rho(\mathbf{r}_c)$	2.4	3.9	5.5			1.1
ϵ	0.18	0.11	0.005			
$H(\mathbf{r}_c)$	−0.03	−0.10	−0.18			
$G(\mathbf{r}_c)/\rho(\mathbf{r}_c)$	0.71	1.00	1.07			
			$Y[AlEt_4]_3$			
r(A−B)	2.57	2.14	2.01	1.56	1.54	
$\rho(\mathbf{r}_c)$	0.24	0.38	0.51	1.46	1.50	0.15
$\nabla^2\rho(\mathbf{r}_c)$	2.5	3.8	5.2	−10.4	−11.3	0.9
ϵ	0.32	0.05	0.02	0.04	0.04	
$H(\mathbf{r}_c)$	−0.02	−0.11	−0.17	−1.10	−1.16	
$G(\mathbf{r}_c)/\rho(\mathbf{r}_c)$	0.80	0.98	1.04	0.26	0.25	

[a] Units: r in Å, $\rho(\mathbf{r})$ in e Å^{-3}, $\nabla^2\rho(\mathbf{r})$ in e Å^{-5}, $H(\mathbf{r})$ in hartree Å^{-3}, $G(\mathbf{r})/\rho(\mathbf{r})$ in hartree e^{-1}. [b] Calculated values (BPW91/II) for the C−C bond are as follows. For C_2H_6: r(C−C) = 1.537 Å; $\rho(\mathbf{r}_c) = 1.55$ e Å^{-3}; $\nabla^2\rho(\mathbf{r}_c) = -12.4$ e Å^{-5}; $H(\mathbf{r}_c) = -1.23$ hartree Å^{-3}; $G(\mathbf{r}_c)/\rho(\mathbf{r}_c) = 0.23$ hartree e^{-1}, $\epsilon = 0.00$. For the $C_2H_5^-$ anion: r(C−C) = 1.548 Å; $\rho(\mathbf{r}_c) = 1.47$ e Å^{-3}; $\nabla^2\rho(\mathbf{r}_c) = -10.44$ e Å^{-5}; $H(\mathbf{r}_c) = -1.17$ hartree Å^{-3}; $G(\mathbf{r}_c)/\rho(\mathbf{r}_c) = 0.30$ hartree e^{-1}; $\epsilon = 0.13$. [c] Taken from ref 4a.

on the basis of the topological parameters the Y···C$_b$ bond ($G(\mathbf{r}_c)/\rho(\mathbf{r}_c) = 0.8$ hartree e^{-1}) seems to be established at the expense of a significantly weakened bridging $Al-C_b$ bond.[34,35]

The contour map of the Laplacian shown in Figure 7b also reveals significant polarization of the outer shell of the core of the Y atom.[36] This result also supports our conclusion that the aluminate bonding shows a significant degree of covalency. Thus, the aluminate bonding is even strong enough to polarize the valence shell of the metal center. Figure 7a reveals polarization of the outer shell of the core of the Y atom of **6** in detail: five charge concentrations (CCs) form a slightly distorted trigonal-bipyramidal polyhedron. The six bridging methyl groups are thus adjacent to the six faces of the trigonal bipyramid of CCs.[37,38]

(iii) Polyagostic Ln···H−C Bonding? As shown in Figure 8, the Y···R−Al fragment (R = Me, Et) in **5** and

(34) In addition to the topological parameters at the bond critical point ($\rho(\mathbf{r}_c)$, $\nabla^2\rho(\mathbf{r}_c)$, and ϵ), the electronic kinetic energy density, $G(\mathbf{r}_c)$, and the total electronic energy density, $H(\mathbf{r}_c)$, at this point can be used to gain a deeper insight into the nature of chemical bonding.[35] It is well-documented[35] that both the ratio $G(\mathbf{r}_c)/\rho(\mathbf{r}_c) < 1$ and $H(\mathbf{r}_c) < 0$ characterize a shared interaction (covalent bonds), while for a closed-shell (or unshared) interaction (ionic, hydrogen, or van der Waals bonds) the value of $G(\mathbf{r}_c)/\rho(\mathbf{r}_c)$ is found to be greater than unity.

(35) (a) Cremer, D.; Kraka, E. *Croat. Chem. Acta.* **1984**, *56*, 1259−1281. (b) Cremer, D.; Kraka, E. *Angew. Chem.* **1984**, *96*, 612−613; *Angew. Chem., Int. Ed. Engl.* **1984**, *23*, 627−628.

(36) As already noted by Bader and co-workers, the shell structure for elements beyond argon in the periodic table is not fully represented by the Laplacian. Thus, only four shells instead of five were observed for the Y metal center $[Kr]5s^24d^1$. We have therefore used the expression "polarization of the outer shell of the core of the Y atom" to account for the occurrence of CPs in the fourth shell of the Y atom. However, valence shell electrons and outer core electrons, as defined by the orbital model, cannot be distinguished on the basis of the Laplacian for elements beyond argon (see, e.g.: Sagar, R. P.; Ku, A. C. T.; Smith, V. H., Jr.; Simas, A. M. *J. Chem. Phys.* **1988**, *88*, 4367−4374). Indeed, studies comparing the results of calculations using all-electron basis sets or effective core potentials have clearly demonstrated that the occurrence of CPs in the outer shell of elements beyond argon has to be attributed mainly to a polarization of the valence electrons and outer core electrons (MacDougall, P. J.; Hall, M. B. *Trans. Am. Crystallogr. Assoc.* **1990**, *26*, 105−123. Bader, R. F. W.; Gillespie, R. J.; Martin, F. *Chem. Phys. Lett.* **1998**, *290*, 488−494).

Downloaded by CARLI CONSORTIUM on June 29, 2009
Published on August 18, 2001 on http://pubs.acs.org | doi: 10.1021/om0102091

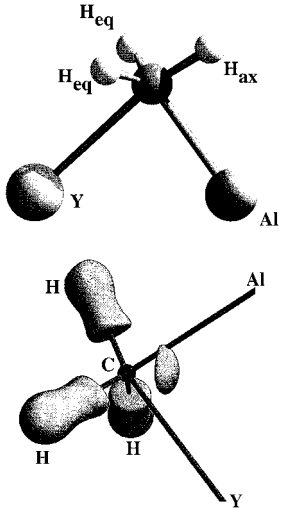

Figure 8. (a, top) μ,η^2-Bridging methyl groups in **5**. Important distances (Å) and angles (deg) (averaged values; corresponding values for **6** are shown in brackets): Y−C = 2.550 [2.570], C−Al = 2.126 [2.137], C−H_{eq} = 1.110 [1.116], C−H_{ax} = 1.106; ∠Y−C−H_{eq} = 84.0 [73.3], ∠Y−C−H_{ax}(Cb) = 168.8 [175.4], ∠Al−C−H_{eq} = 124.1 [119.1], Al−C−H_{ax}(C_β) = 86.9 [101.4], ∠Y−C−Al = 82.4 [83.0], ∠H_{eq}−C−H_{eq} = 107.9 [106.5], H_{eq}−C−H_{ax}(C_β) = 102.2 [104.3], τ(Y···Al−C−H_{ax}(C_β) = 176.6 [178.5]. (b, bottom) Isovalue envelope plot of the Laplacian of the electron density ($\nabla^2\rho(\mathbf{r}) = -10$ e Å^{-5}) showing the μ,η^2-bridging methyl group in **5**.

6 closely conforms to local C_s symmetry. The geometry of the bridging C atom is best described as a distorted trigonal bipyramid with two hydrogen atoms (H_{eq}) and the Al atom forming the equatorial plane. Two equatorial H atoms establish remarkably short Y···H contacts of 2.343 and 2.495 Å, respectively, which have been interpreted in the literature as *polyagostic* interactions.[4a] However, as in the neutron diffraction study of $Nd[AlMe_4]_3$, no significant C−H bond activation attends the short Y···H contacts: C−H_{eq} = 1.110 Å and C−H_{ax} = 1.106 Å in **5**. Despite the acute Y−C−H_{eq} angles of 84.0 and 73.3° in **5** and **6**, respectively, no Y···H bond CP signaling a pronounced agostic interaction can be identified on the basis of a topological analysis. The rather different Y−C−H_{eq} angles in **5** and **6** clearly suggest that the acute angles are a geometrical consequence of the hypervalent character of the bridging C atoms. Comparing the geometrical situation in **5** and **6**, the sterically more demanding ethyl group affords a significantly larger ∠Al−C−X (X = Me, H_{ax}) angle of 101.4° vs 86.9°, respectively. As a consequence, the H_{eq} atoms are tilted further toward the Y center in **6** in order to maintain the H_{eq}−C−X angle of 104.3° in the same range as in **5** (102.2°). The rather invariant H_{eq}−C−X angles in **5** and **6** suggest that the CH_2X groups should be described as methanide/ethanide anions, with the charge of the lone pair equally shared between the Lewis acidic Al and Y metal centers. The envelope plot of the Laplacian of the electron density (Figure 8b) clearly shows the local charge concentration, which formally corresponds to a lone pair in the Lewis model on the C atom of the methanide group in **5**.

Conclusion

Previously, aluminum compounds have been ascribed various roles in metallocene-based α-olefin polymerization including that of (i) a scavenger (of moisture), (ii) an alkylating reagent, (iii) a chain transfer reagent, and (iv) a stabilizing counterion of the active species.[7,8] It is interesting to note that the catalytic activity of cationic zirconocene complexes markedly depends on the alkyl group R attached to the cocatalyst system AlR_3 and alumoxane, respectively. For example, the sterically most hindered system $Cp^*_2ZrCl_2$/Al*i*Bu_3 gave the highest activity in ethylene polymerization compared to the $AlMe_3$, $AlEt_3$, or MAO (methylalumoxane) congeners.[40] Given the present structural and theoretical evidence of various aluminate coordination modes, one is tempted to speculate on an even more multifaceted role of aluminate/MAO bonding in α-olefin polymerization. Supposedly, aluminate bonding/nonbonding in cationic zirconocene complexes is involved in the formation of dormant, polymerization-retarding species ("resting state") and the polymerization-active separated ion pair, respectively (Scheme 3).[7,41,42] Tetraalkylaluminate formation arises also from commercially available MAO, which contains a considerable amount of associated ($MAO{\cdot}AlMe_3$) and free trimethylaluminum (Al_2Me_6).[43]

Strongly μ,η^3-binding aluminate ligands ($\eta^2 \rightarrow \eta^3$ = −8 kcal/mol) such as established in this work might significantly affect the steady-state reactions involving polymerization-retarding aluminate complexes (species II and III in Scheme 3). For comparison, the intramolecular Ln···(olefin) binding energy in $Cp^*_2Y[\eta^1{:}\eta^2$-$CH_2CH_2CH_2CH{=}CH_2]$ was estimated as 10.4 kcal/mol on the basis of a variable-temperature NMR investigation,[44] which is also supported by theoretical investigations.[45] Watson and Herskovitz previously reported that $AlMe_3$ binds even more strongly than THF to the precatalyst system $[Cp^*_2LuCH_3]$ and in low excess completely stops ethylene polymerization.[46] Moreover, recent investigations of lanthanide(II,III)-based initiators such as $[Cp^*_2Yb(AlH_3)(NEt_3)]$[47] and $[Me_2Si(C_5Me_4)_2]$-$La(AlMe_4)$[48] revealed that the presence of aluminum

(37) We note that in the case of **5** even *six* local charge concentrations are observed. It remains to be clarified whether the different numbers of these domains (six in **5** and five in **6**) and their mutual arrangements are a consequence of the different bridging groups (methyl vs ethyl) attached to the Y center. Indeed, the calculated Y−C bond distances in **5** are ∼0.02 Å shorter than those in **6**, suggesting a stronger Y−C bonding in **5**. Thus, the ligand-induced charge polarization in **5** might be more pronounced compared with **6**, causing the formation of *six* CCs in **5** vs. *five* CCs in **6**.

(38) We note that in the case of **5** six CCs form a slightly distorted trigonal antiprism.

(39) (a) Scherer, W.; Hieringer, W.; Spiegler, M.; Sirsch, P.; McGrady, G. S.; Downs, A. J.; Haaland, A.; Pedersen, B. *Chem. Commun.* **1998**, 2471−2472. (b) Popelier, P. L. A.; Logothetis, G. *J. Organomet. Chem.* **1998**, *555*, 101−111.

(40) Resconi, L.; Giannini, U.; Albizzati, E.; Piemontesi, F. *Polym. Prepr. Jpn.* **1991**, *32*, 463−464.

(41) Tritto, I.; Donetti, R.; Sacchi, M. C.; Locatelli, P.; Zannoni, G. *Macromolecules* **1997**, *30*, 1247−1252 and references therein.

(42) Vanka, K.; Chan, M. S. W.; Pye, C. C.; Ziegler, T. *Organometallics* **2000**, *19*, 1841−1849.

(43) (a) Barron, A. R. *Organometallics* **1995**, *14*, 3581−3583. (b) Tritto, I.; Sacchi, M. C.; Locatelli, P.; Li, S. X. *Macromol. Chem. Phys.* **1996**, *197*, 1537−1544.

(44) Casey, C. P.; Hallenbeck, S. L.; Wright, J. M.; Landis, C. R. *J. Am. Chem. Soc.* **1997**, *119*, 9680−9690.

(45) (a) Margl, P.; Deng, L.; Ziegler, T. *Organometallics* **1998**, *17*, 933−946. (b) Koga, N. *Theor. Chim. Acta* **1999**, *102*, 285−292.

(46) Watson, P. L.; Herskovitz, T. *ACS Symp. Ser.* **1983**, *No. 212*, 459−479.

(47) Knjazhanski, S. Ya.; Elizalde, L.; Cadenas, G.; Bulychev, B. M. *J. Organomet. Chem.* **1998**, *568*, 33−40.

Downloaded by CARLI CONSORTIUM on June 29, 2009
Published on August 18, 2001 on http://pubs.acs.org | doi: 10.1021/om0102091

Scheme 3. Mechanistic Scenario of Zirconocene-Mediated Ethylene Polymerization[a]

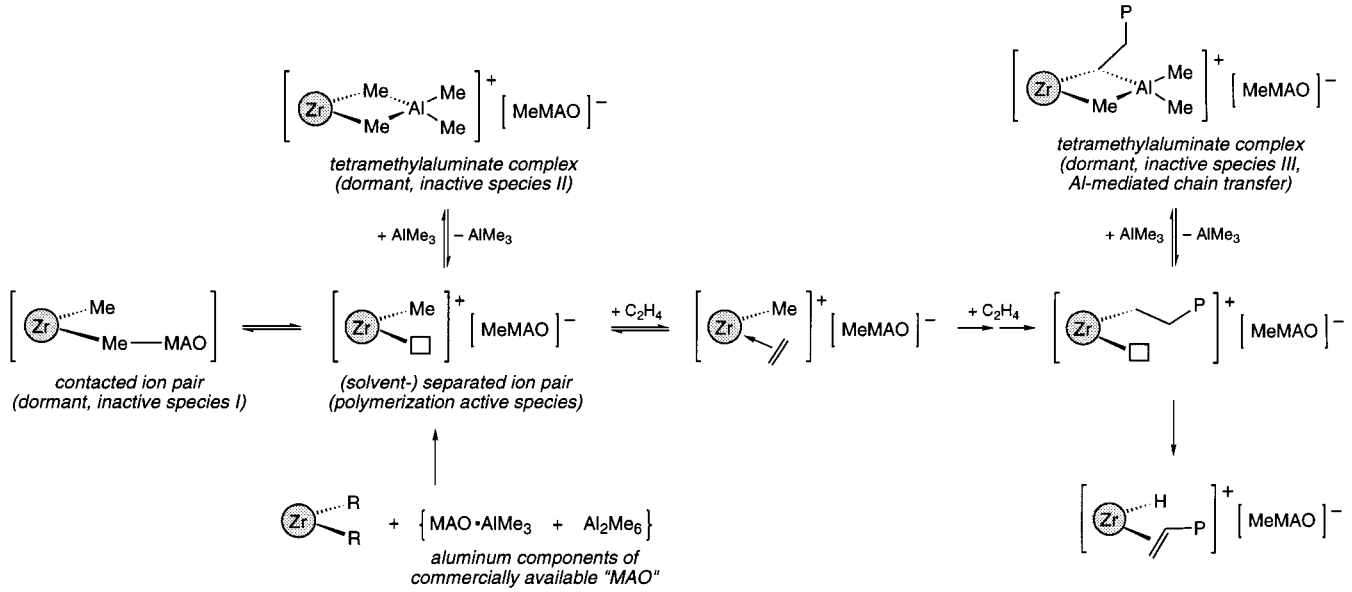

[a] The coordinated solvent is not shown. □ denotes a vacant coordination site. The contact ion pair is often formulated as oxygen (MeMAO)-bridged species.

components decisively affects catalytic activity, molecular weight distribution, and stereospecificity in acrylate polymerization. Organolanthanide complexes, predominantly metallocene derivatives of type Cp^*_2LuR (R = alkyl), have already been proven to be excellent models for clarifying the active sites of Ziegler−Natta catalysts, i.e., $[Cp^*_2ZrR]^+$ (R = alkyl), by emulation of the major initiation, propagation, and termination steps which revealed key features such as insertion, β-hydrogen elimination, and β-alkyl elimination via CH activation and σ-bond metathesis processes.[49] Organolanthanide complexes, predominantly aluminate derivatives, could also shed more light on the action of organoaluminum-derived cocatalysts, i.e., their role of inhibitors vs promoters, in so-called "single site" metallocene initiators for α-olefin polymerization.

Experimental Section

General Considerations. All air- and moisture-sensitive compounds were manipulated with the rigorous exclusion of oxygen and moisture in flame-dried (180 °C) Schlenk-type glassware using standard high-vacuum techniques or an argon-filled glovebox (MBraun) with O_2/H_2O < 1 ppm. The solvents were predried, distilled from Na/K alloy, and stored in a glovebox. Deuterated solvents were obtained from Deutero GmbH and degassed and dried over Na/K alloy.

Trimethyl-, triethyl-, and triisobutylaluminum were purchased from Aldrich and used as received. $Yb[N(SiMe_3)_2]_2(THF)_2$ (**1**) was synthesized from $YbI_2(THF)_{2.5}$ and $K[N(SiMe_3)_2]$ according to common salt metathesis procedures and recrystallized prior to use.[20] NMR spectra were recorded either on a Bruker DPX-400 (FT; 400 MHz for ^{1}H, 100 MHz for ^{13}C) or on a JEOL JNM-GX-400 (FT; 400 MHz for ^{1}H, 100 MHz for ^{13}C) spectrometer. ^{1}H and ^{13}C NMR shifts are referenced to internal solvent resonances and reported relative to TMS. IR spectra were recorded on a Perkin-Elmer 1650-FTIR spectrometer as Nujol mulls. Elemental analyses were performed in the microanalytical laboratory of the institute.

Bis(tetramethylaluminato)ytterbium(II) (2). In a glovebox, **1** (0.319 g, 0.5 mmol) was dissolved in 15 mL of *n*-hexane. After addition of excess trimethylaluminum (0.29 mg, 8 mmol) diluted in 5 mL of *n*-hexane, the initially orange solution immediately turned pale yellow, forming a slight yellow precipitate. The reaction mixture was stirred for 2 h at ambient temperature and then centrifuged, leaving a pale yellow precipitate and a clear colorless solution. The precipitate was washed several times with 5 mL of *n*-hexane to yield **2** as a pale yellow powder in almost quantitative yield (165 mg, >95%). Compound **2** is insoluble in aliphatic and aromatic hydrocarbons and decomposes upon addition of donating solvents. IR (Nujol, cm^{-1}): 1210 m, 1172 w, 1053 m, 702 s, 614 m, 590 w, 528 w. Anal. Calcd for $C_8H_{24}Al_2Yb$: C, 27.67; H, 6.97. Found: C, 27.15; H, 6.60.

Bis(tetraethylaluminato)ytterbium(II) (3). In a glovebox, excess triethylaluminum (4 mmol, 4 mL of a 1M solution in *n*-hexane) was added to **1** (0.139 g, 0.5 mmol) dissolved in 10 mL of *n*-hexane. Within 5 min the initially orange solution turned yellow while forming a small amount of a pale yellow precipitate. After it was stirred for 2 h at ambient temperature, the reaction mixture was centrifuged, leaving <0.01 g of the pale yellow precipitate. The intensely yellow solution was cooled to −40 °C, yielding compound **3** as yellow needles (0.160 g, 69%). IR (Nujol, cm^{-1}): 1170 w, 946 m, 653 s, 523 w. Anal. Calcd for $C_{16}H_{40}Al_2Yb$: C, 41.82; H, 8.77. Found: C, 43.73; H, 9.21. ^{1}H NMR (C_6D_6, 25 °C, ppm): 1.28 (t, ^3J(H,H) = 7.7 Hz, 3H, CH_3); 0.09 (q, ^3J(H,H) = 7.7 Hz, 2H, CH_2). ^{13}C NMR (C_6D_6, 25 °C, ppm): 11.0 (*C*H$_3$); 6.7 (*C*H$_2$).

Bis(tetraisobutylaluminato)ytterbium(II) (4). In a glovebox, excess triisobutylaluminum (4 mmol, 4 mL of a 1 M solution in *n*-hexane) was added to **1** (0.139 g, 0.5 mmol) dissolved in 10 mL of *n*-hexane. Within 30 min the initially orange solution turned dark yellow while forming a small amount of a brown precipitate. After it was stirred for 15 h at ambient temperature, the reaction mixture was centrifuged, leaving <0.03 g of a brown precipitate. After evaporation of half of the solvent, crystallization at −40 °C yielded compound **4** as dark yellow rodlike crystals (0.210 g, 62%). IR (Nujol, cm^{-1}): 2725 m, 1158 w, 1066 w, 674 m. Anal. Calcd for $C_{32}H_{72}Al_2Yb$: C, 56.20; H, 10.61. Found: C, 54.75; H, 10.48. ^{1}H NMR (C_6D_6, 25 °C, ppm): 1.95 (sp, ^3J(H,H) = 4.5 Hz, 1H, C*H*); 1.13 (d, ^3J(H,H) = 4.2 Hz, 6H, CH_3); 0.43 (d, ^3J(H,H) = 4.7 Hz, 2H,

(48) (a) Anwander, R.; Görlitzer, H. W. Unpublished results. (b) Görlitzer, H. W. Ph.D. Thesis, Technische Universität München, 1999.

(49) (a) Watson, P. L.; Parshall, G. W. *Acc. Chem. Res.* **1985**, *18*, 51−56. (b) Burger, B. J.; Cotter, W. D.; Coughlin, E. B.; Chacon, S. T.; Hajela, S.; Herzog, T. A.; Köhn, R.; Mitchell, J.; Piers, W. E.; Shapiro, P. J.; Bercaw, J. E. In *Ziegler Catalysts*; Fink, G., Mühlhaupt, R., Brintzinger, H.-H., Eds.; Springer-Verlag: Berlin, 1995; pp 317−331.

Downloaded by CARLI CONSORTIUM on June 29, 2009
Published on August 18, 2001 on http://pubs.acs.org | doi: 10.1021/om0102091

CH_2). ^{13}C NMR (C_6D_6, 25 °C, ppm): 29.8 (CH_2); 28.9 (CH); 28.3 (CH_3).

X-ray Crystal Structure Determination of 3. Yellow well-shaped cubic (0.2 × 0.2 × 0.2 mm) crystals of **3** were obtained via fractional crystallization at −35 °C from *n*-hexane. X-ray data were collected on a kappa-CCD system from Nonius with a rotating-anode X-ray generator (Nonius FR591; Mo K_α, $\lambda = 0.710\ 73$ Å) using both ω and ϕ scans with $\Delta\phi = \Delta\omega = 1°$.[50a] The unit cell was determined from 57 267 reflections. The intensities were first corrected for beam inhomogeneity, crystal decay, Lorentz and polarization effects, and anomalous dispersion by the program SCALEPACK[50b] using a tight scale restraint (0.002). An empirical absorption correction was then applied ($T_{min} = 0.350(9)$, $T_{max} = 0.420(11)$), and symmetry-equivalent and multiply measured reflections were averaged with the program SORTAV.[51] Crystal data are as follows: formula, $C_{32}H_{80}Al_4Yb_2$; $M_r = 918.96$; trigonal; space group $P3_2$ (No. 145); $a = 11.7410(1)$ Å, $c = 27.3370(2)$ Å, $V = 3263.56(5)$ Å^3; $T = 243(1)$ K; $Z = 3$; $F(000) = 1392$; $\rho_{calcd} = 1.403$ g/cm^3; $\mu = 4.4$ mm^{-1}. A total of 57 267 reflections were collected at a detector distance of 40 mm ($6.0° < 2\theta < 55.0°$, h (−15 to +15); k (−15 to +15); l (−35 to +35)) and merged ($R_{int}(F_o^2) = 0.052$) to give 9872 unique reflections (9750 observed reflections ($I > 2\sigma(I)$)) which were used in the full-matrix refinement of 407 parameters.[52] All non-hydrogen atom positions were refined freely with anisotropic thermal parameters for non-hydrogen atoms. The positions of the agostic hydrogen atoms were refined freely, while nonagostic hydrogen atoms were fixed at calculated positions. The isotropic thermal displacement parameters of all hydrogen atoms were related to the parent carbon atom; $U_{iso}(H) = 1.5[U_{eq}(C)]$. The structure refinement of F_o^2 data converged at shift/error <0.0001: R1 = 0.0241, wR2 = 0.0595, GOF = 1.08; Flack parameter 0.05(1); residual electron density +0.90/−0.84 e Å^{-3}. Scattering factors and anomalous dispersion corrections were taken from ref 53. All figures were prepared using the programs PLATON[54] and SCHAKAL.[55]

DFT Calculations. All theoretical calculations were carried out with the GAUSSIAN-98 suite of programs.[56] The Becke exchange functional[57] and the Perdew−Wang correlation functional[58] (BPW91) are employed in all DFT calculations. Our standard basis set (denoted "I") uses quasi-relativistic effective core potentials (ECP) to replace the 60 and 59 innermost electrons of the Yb(II) and Yb(III) atoms, respectively.[59] The f orbitals were treated within the core orbitals with a fixed 4f occupation corresponding to the desired valency of the Yb atom (II or III). The outermost 5s, 5p, 5d, and 6s valence orbitals for Yb have been replaced by the optimized (7s6p5d)/[5s4p3d] valence basis set.[59] All-electron polarized double-ζ 6-31G(d) basis sets were employed for the H,[60a] C,[60b] and Al[60c] atoms. For the all-electron calculations, double-ζ DZVP basis sets[61] were employed for Y, Al, C, and H atoms in all ytterbium compounds. This basis set was denoted "II".

Full geometry optimizations of the $YbMe_2$ and $YbMe_3$ model systems were carried out without any symmetry constraints. However, the optimized structures of $YbMe_2$ and $YbMe_3$ correspond to the C_2 and C_3 symmetries, respectively. Frequency calculations performed for the fully optimized structures of $YbMe_2$ and $YbMe_3$ showed no imaginary frequencies. Geometry optimizations for the $Yb[AlEt_4]^+$ cation and the $Yb[AlEt_4]_3^-$ anion species were carried out without symmetry constraints. The final optimization of the $Yb[AlEt_4]_3^-$ anion was made assuming C_3 symmetry, and a negligible energy difference between the constrained (C_3) and unconstrained (C_1) models of the $Yb[AlEt_4]_3^-$ anion was found.

Frequency calculations were performed for the **3a** (D_{2d}) and **3c** (C_1) model systems. Corresponding optimized structures were found to be the second-order saddle points with two imaginary frequencies for each of the model systems. Vibrational analysis of the nearly converged (with respect to the default threshold values used in GAUSSIAN-98) structures of **5** (C_3) and **6** (C_3) species were not carried out. However, all forces with respect to the default threshold on all the nuclei in **5** and **6** vanish, thus justifying the applicability of a topological analysis of the electron density within the AIM theory framework.

The GIAO (gauge-including atomic orbital) method was employed to calculate the ^1H and ^{13}C NMR shielding tensors for the **3a** and **3c** model systems. ^1H and ^{13}C NMR chemical shifts are reported with respect to the calculated (BPW91/6-31G(d)) isotropic shielding constants $\sigma(^1H)$ of 31.85 ppm and $\sigma(^{13}C)$ of 189.10 ppm of TMS, respectively. The calculation on TMS was carried out assuming staggered T_d symmetry.

The topological analyses of the theoretical electron densities were carried out using the AIMPAC software package.[32b]

All contour plots were produced using the programs written in our laboratory. All 3-D isovalue surface plots were prepared with XDGRAPH from the XD software package.[62]

Acknowledgment. M.T. thanks the Alexander von Humboldt Foundation for a Postdoctoral Fellowship. Generous support from Deutsche Forschungsgemeinschaft and Prof. W. A. Herrmann is gratefully acknowledged.

Supporting Information Available: Tables of crystal data, structure solution and refinement, atomic coordinates, bond lengths and angles, and anisotropic thermal parameters for **3**, a table of the calculated ^1H and ^{13}C NMR chemical shifts, a graphical representation of the variable-temperature NMR study, and 2-D and 3-D plots of the ELF for **5** and **6**. X-ray crystallographic data, in CIF format, are also available. This material is available free of charge via the Internet at http://pubs.acs.org.

OM0102091

Downloaded by CARLI CONSORTIUM on June 29, 2009
Published on August 18, 2001 on http://pubs.acs.org | doi: 10.1021/om0102091

(50) (a) "Collect" data collection software; Nonius BV, Delft, The Netherlands, 1998. (b) Otwinowski, Z.; Minor, W. Processing of X-ray Diffraction Data Collected in Oscillation Mode. *Methods in Enzymology*; Carter, C. W., Jr., Sweet, R. M., Eds.; Academic Press: San Diego, CA, 1997; Volume 276, Macromolecular Crystallography, Part A, pp 307−326.

(51) Blessing, R. H. *Acta Crystallogr.* **1995**, *A51*, 33−38.

(52) Sheldrick, G. M. SHELXL97: a Program for Crystal Structure Refinement; University of Göttingen, Göttingen, Germany, 1997.

(53) *International Tables for Crystallography*; Wilson, A. J. C., Ed.; Kluwer Academic: Dordrecht, The Netherlands, 1992; Vol. C, Tables 6.1.1.4 (pp 500−502), 4.2.6.8 (pp 219−222), and 4.2.4.2 (pp 193−199),

(54) Spek, A. L. *Acta Crystallogr.* **1990**, *A46*, C-34.

(55) Keller, E. SCHAKAL; Crystallographic Institute, University of Freiburg, Freiburg, Germany, 1988.

(56) Frisch, M. J.; Trucks, G. W.; Schlegel, H. B.; Scuseria, G. E.; Robb, M. A.; Cheeseman, J. R.; Zakrzewski, V. G.; Montgomery, J. A., Jr.; Stratmann, R. E.; Burant, J. C.; Dapprich, S.; Millam, J. M.; Daniels, A. D.; Kudin, K. N.; Strain, M. C.; Farkas, O.; Tomasi, J.; Barone, V.; Cossi, M.; Cammi, R.; Mennucci, B.; Pomelli, C.; Adamo, C.; Clifford, S.; Ochterski, J.; Petersson, G. A.; Ayala, P. Y.; Cui, Q.; Morokuma, K.; Malick, D. K.; Rabuck, A. D.; Raghavachari, K.; Foresman, J. B.; Cioslowski, J.; Ortiz, J. V.; Stefanov, B. B.; Liu, G.; Liashenko, A.; Piskorz, P.; Komaromi, I.; Gomperts, R.; Martin, R. L.; Fox, D. J.; Keith, T.; Al-Laham, M. A.; Peng, C. Y.; Nanayakkara, A.; Gonzalez, C.; Challacombe, M.; Gill, P. M. W.; Johnson, B. G.; Chen, W.; Wong, M. W.; Andres, J. L.; Head-Gordon, M.; Replogle, E. S.; Pople, J. A. *Gaussian 98*, revision A.7; Gaussian, Inc.: Pittsburgh, PA, 1998.

(57) Becke, A. D. *Phys. Rev.* **1988**, *A38*, 3098−3100.

(58) Perdew, J. P.; Wang, Y. *Phys. Rev.* **1992**, *B45*, 13244−13249.

(59) Dolg, M.; Stoll, H.; Savin, A. *Theor. Chim. Acta* **1989**, *75*, 173−194.

(60) (a) Hehre, W. J.; Ditchfield, R.; Pople, J. A. *J. Chem. Phys.* **1972**, *56*, 2257−2261. (b) Hariharan, P. C.; Pople, J. A. *Theor. Chim. Acta* **1973**, *28*, 213−222. (c) Francl, M. M.; Petro, W. J.; Hehre, W. J.; Binkley, J. S.; Gordon, M. S.; DeFree, D. J.; Pople, J. A. *J. Chem. Phys.* **1982**, *77*, 3654−3665.

(61) Godbout, N.; Salahub, D. R.; Andzelm, J.; Wimmer, E. *Can. J. Chem.* **1992**, *70*, 560−571.

(62) Koritsanszky, T.; Howard, S. T.; Su, Z.; Mallinson, P. R.; Richter, T.; Hansen, N. K. XD, Computer Program Package for Multipole Refinement and Analysis of Electron Densities from Diffraction Data; Free University of Berlin, Berlin, Germany, June 1997.